May 1982 LRP 204/82

PLASMA SURFACE INTERACTIONS IN THE TCA TOKAMAK: A PRELIMINARY STUDY USING DEPOSITION PROBES

PROJECT REPORT 1981

J. K. Gimzewski, B. Braun, R.J. Brewer, S. Veprek,

H. Stüssi and F. Hofmann

collaboration between :

Institute of Inorganic Chemistry
University of Zurich

Institute of Physics
University of Zurich

and

Centre de Recherches en Physique des Plasmas
Association Euratom - Confédération Suisse
Ecole Polytechnique Fédérale de Lausanne

PLASMA-SURFACE INTERACTIONS IN THE TCA TOKAMAK:

A PRELIMINARY STUDY USING DEPOSITION PROBES

PROJECT REPORT 1981

J.K. Gimzewski, B. Braun+, R.J. Brewer and S. Veprek

Institute of Inorganic Chemistry
University of Zurich
Winterthurerstrasse 190
CH-8057 ZURICH

H. Stüssi

Institute of Physics
University of Zurich
Schönberggasse 9
CH-8001 ZURICH

and

F. Hofmann

Centre de Recherches en Physique des Plasmas
Association Euratom - Confédération Suisse
Ecole Polytechnique Fédérale de Lausanne
CH-1007 LAUSANNE

+ On leave from Research Institute of Physics
S-10405 STOCKHOLM

ABSTRACT

XPS and RBS measurements of deposition probes which were exposed to the TCA Tokamak plasma, in the shadow of the limiter, have been performed. Based on a quantitative analysis of these data the impurity fluxes in the scrape-off region of the plasma are determined. Radial profiles of the deposition thickness from two angular positions on the torus were measured to obtain some information on the homogeneity of the impurity fluxes.

TABLE OF CONTENTS

1. INTRODUCTION AND OBJECTIVES

2. EXPERIMENTAL

2.1 The Samples
2.2 XPS Analysis
2.3 Sample Exposure in TCA
2.4 Rutherford Backscattering
2.5 XPS Analysis: Data Reduction Methods

3. RESULTS AND DISCUSSION

3.1 Sapphire Samples: Survey Spectra Analysis
3.2 Sapphire Samples: Deposit Thickness Determination
3.3 Stainless Steel Samples: Substrate Compositional Changes
3.4 XPS Analysis of the Deposit
3.5 Chemical Environment of the Species Deposited

4. CONCLUDING REMARKS

1. INTRODUCTION AND OBJECTIVES

The use of deposition probes is an important method for the characterization of impurity fluxes in the boundary layer of Tokamak plasmas. In a recent review by McCracken and Stott {1} three major categories of surface science information were considered desirable as regards plasma-surface interactions in Tokamaks:

(a) Surface Structure,
(b) Surface Composition, and
(c) Depth Distribution of Deposited or Implanted Material.

The objectives of the present work are to study surface-compositional changes and depth distributions for samples exposed to a plasma in the TCA Tokamak (TCA) {2}. X-Ray Photoelectron Spectroscopy (XPS) and Rutherford Backscattering Spectroscopy (RBS) were chosen as analysis techniques for this study because of the quantitative accuracy of the latter method, and the elemental detection range and the surface sensitivity of the former method. The comparative analysis by electron spectroscopic and RBS techniques have been discussed by Howard et al. {3}.

Surface studies at PLT {4} have shown that the principal impurity at the radius of the ring limiter is iron. In similar investigations at ATC {5} and PULSATOR {6} it has been concluded that the wall condition is determined by the deposition of metallic particles during discharges and by absorption of residual gases between discharges. It has been established that metallic impurities are present in the scrape-off layer of most Tokamak devices {4-8}.

The mechanisms responsible for transport of the metallic impurities are not well understood. Self-sputtering by the wall material, oxygen and ion-sputtering, and unipolar arcing have been considered as potential contributors to the process.

In order to study plasma-surface processes occuring in the TCA-Tokamak, probes made of the wall material (316 LN stainless steel)

were used to study surface compositional changes that occured upon exposure of the wall to the plasma and sapphire deposition probes were used to assess the contribution of deposition of impurities from the plasma. The latter measurement provides information on the amount and composition of the impurity deposited from the plasma and the former measurement provides preliminary information for a feasibility study on the use of experimenal probes to study plasma-surface interactions in a Tokamak environment. Future studies will be of a more detailed nature using a vacuum-lock sample transfer mechanism.

2 EXPERIMENTAL

2.1 The Samples

Sample materials used for this study were 316LN stainless steel and sapphire of dimensions 50x10x0,5 mm. The samples were attached to a probe mount based on a NW35CF flange (Fig. 1).

Each probe unit was comprised of a stainless steel and a sapphire sample. The geometry of the probe in relation to the Tokamak's radial dimensions is shown in figure 2. The probes were oriented to have the directions of the electron and ion currents perpendicular to the sample surfaces. In the following sections probe surfaces oriented to have the directions of the electron current perpendicular to the sample are called electron-exposed and for the ion-current direction they are called ion-exposed.

Two NW35CF ports, situated in the equatorial plane of the vacuum vessel, at angular positions defined between sectors 7 and 8 (7,8) and between sectors 16 and 17 (16,17) were used (Fig. 3). These positions. on the outer circumference of the vessel, may be related to the limiter, which is in sector 9. During the experiments, ions were limited to an anticlockwise rotation and electrons to a clockwise rotation, as viewed from above the torus. With respect to the ion flux. samples (7,8) were in the proximity of the limiter and samples (16,17) were

situated at ~ 180° from the limiter. This arrangement permitted a limited investigation of the angular homogeneity of the impurity fluxes.

The deposition dependence upon radial distance, Z, which is defined in figure 1, was also investigated. This distance is related to the distance from the plasma edge as defined by the limiter, d, by:

$$d = 110 - Z \text{ (mm)}. \tag{1}$$

Sample pretreatment and cleaning were carried out at EIR-Würenlingen and at ACI-University of Zurich.

For the 316LN stainless steel samples, preparation consisted of the following procedure:

(a) Electrolytic polishing in an aqueous solution of H_2SO_4/H_3PO_4 and glycerol

(b) Vacuum annealing at 700°C for c.a. 2 hours

(c) Degreasing in methylene chloride

(d) Cleaning in a 'Deconex' solution at ~ 100°C for c.a. 20 minutes

(e) Rinsing in deionized water at ~ 100°C for c.a. 20 minutes

(f) Drying in air at ~ 20°C

The samples were then mounted in the holder.

Sapphire samples were subjected to parts (c)-(f) of the procedure above prior to being mounted in the holder.

The probe holders were mounted on a NW35CF crosspiece which was equipped with a UHV valve. This unit was connected to a UHV vacuum system and the entire system was baked overnight at ~ 400°C under a vacuum of ~ 10^{-8} mb.

Prior to transport, the unit was pressurized with Argon (99,999% purity) to atmospheric pressure and the unit was sealed using the valve. The unit was removed and transported to the TCA site where the probes were mounted onto the Tokamak vacuum vessel under atmospheric conditions. Care was taken to minimize the exposure time of the samples to the atmosphere.

After exposure to the TCA plasma for a time dependent on operating conditions, the samples were removed under atmospheric conditions and remounted in the crosspiece, which was subsequently flushed with Argon, sealed and transported to Zurich.

Samples were stored under Argon until transfer, under atmospheric conditions, to the XPS <u>or</u> RBS vacuum chambers for analysis.

2.2 XPS Analysis

X-ray Photoelectron Spectroscopy (XPS) was used to determine the elemental composition of the surface regions of the samples. This technique was also used to measure the thickness of the material deposited on the sapphire samples.

A Leybold Heraeus (LHS-10) XPS spectrometer equipped with Al K_α and Mg K_α radiation sources was used for the study. Most of the spectra were recorded in the constant transmission ($\Delta E/E$ = constant) mode. 1000 eV "survey" scans were taken for both the electron- and ion-exposed surfaces at several radial distances Z along the sample surface.

Data was recorded both on an analog X-Y recorder and digitally using a Tracor Northern (TN1750) Multichannel scaler (MCS). The MCS was equipped with a microprocessor which permitted a printed output of the net peak areas of selected regions of the spectrum. The peak areas were determined using a user-selected linear background subtraction.

These data were used for quantitative analysis calculations described in 2.5.

The lateral-spatial resolution of the XPS system is determined by the width of the entrance and exit slits of the hemispherical analyser and by the electron optics of the retarding lens system. The resolution was determined experimentally using a Pt-steel interface and was found to agree with the theoretical value (2mm). This value corresponds to the resolution in the distance Z. The virtual slit length of 10 mm resulted in the analysis being conducted across the full width of the sample.

2.3 Sample Exposure to TCA

Three sets of samples were exposed to the TCA plasma. The preliminary nature of the TCA experiment did not permit a detailed history to be made for each sample set. During the experiments non-uniform operating conditions prevailed and the samples were labelled according to their insertion and removel dates. These samples were:

(a) 26.06.80 - 30.06.80
(b) 30.06.80 - 08.09.80
(c) 08.09.80 - 22.11.80

Sample (a) was discharge cleaned only.

Sample (b) was discharge cleaned and exposed to ~ 100 shots at a maximum current of 80 kA with a shot duration of 80 ms at ~ 60 kA.

Sample (c) was discharge cleaned and exposed to ~ 30 shots at a maximum current of 100 kA with a shot duration of ~ 100 ms.

2.4 Rutherford Backscattering

The sapphire samples were analysed using the RBS technique. 2 MeV $^{4}He^{+}$ projectiles accelerated by a Van de Graaff generator were used for the measurements. Sapphire substrates were not particularly suitable for the measurements because fluorescence and electrostatic charging occured during ion bombardment. These phenomena caused distortion of the spectra. Later measurements were conducted on samples which had been coated with a thin layer of gold prior to analyses. The effect of the gold overlayer was to reduce charging of the sample. However, the inclusion of this thin overlayer did not present problems in data analysis because the gold peak does not overlap with the Fe, Cr or Ni peaks.

The projectiles used in this study did not permit resolution of iron and nickel; however, as can be seen in figure 4, it was possible to partially resolve iron from chromium and thus obtain a semiquantitative estimate of the relative concentration of iron to chromium.

The average overlayer depth of deposit was calculated from the iron, chromium and nickel peaks. The overlayer depth was calculated using a standard procedure in which the average Rutherford cross-sections for Fe, Cr and Ni were used and where the atomic density of the deposit was assumed to be close to that for iron (7,89 g/cm^3). The latter assumption is reasonable insofar as the XPS analysis indicated that the deposit composition resembled that of stainless steel which has a density close to that of iron. The overlayer depth was calculated using the expression:

$$d = \frac{n_{Fe} + n_{Cr} + n_{Ni}}{\rho} , \qquad (2)$$

Where n is the atomic surface concentration in atoms/cm^2 and ρ is the atomic density. The values of n were determined using the expressions:

$$n_{Cr} = 3.125 \times 10^{15} \frac{A_{Cr}}{H_{Al}} \ (at/cm^2), \qquad (3)$$

$$n_{Fe} = 2.6586 \times 10^{15} \frac{A_{Fe}}{H_{Al}} \ (at/cm^2), \qquad (4)$$

and

$$n_{Ni} = 2.2902 \times 10^{15} \frac{A_{Ni}}{H_{Al}} \ (at/cm^2), \qquad (5)$$

where A is the area of the RBS peak for the element which appears in the subscript and H_{Al} is the height of the aluminium edge which served as a calibration signal.

The spot size of the ion beam used in this study is estimated to be 0,2 - 0,3 mm in diameter. This value may be compared with the analysis spot size used in the XPS studies which is ~ 10 mm in length perpendicular to the Z direction and ~ 2 mm wide.

2.5 XPS Analsis: Data Reduction Method

Quantitative analysis of the elements present on the sample surface and subsurface regions were determined from the net peak areas of the most intense photopeaks of each element detected. The atomic percent composition was calculated using the equation:

$$n_i = 100 \ \frac{A_i \cdot K_i^{1,5}}{\sigma_i} \Big/ \sum_j \frac{A_j \cdot K_j^{1,5}}{\sigma_j} \ , \qquad (6)$$

where n_i is the atomic percent composition of element i,

K is the kinetic energy of the photoelectrons,

σ is the photoionization cross-section of the photopeak considered, and

A is the net peak area.

The summation extends over the j elements considered.

Further details of the analysis method are discussed elsewhere {9,10}. Standard photoionization cross-sections were used for an Al K_α radiation excitation source {11}.

The depth of material deposited was determined from the attenuation of the Al 2s and Al 2p photopeak signal on the sapphire samples.

Assuming a smooth uniform overlayer of depth x, the substrate photopeak intensity I' is given by {9}

$$I' = I'_o(1-e^{-x/\Delta' \sin\Theta}) \quad (7)$$

where I'_o is the photopeak intensity for a clean substrate surface,

Δ' is the photoelectron escape depth for the photopeak photoelectrons, and

Θ is the take-off angle.

For the overlayer, the photopeak intensity I is given by

$$I = I_o \, e^{-x/\Delta \sin\Theta} \quad (8)$$

Equations (2) and (3) may be combined to give

$$I' = I'_o \left[1 - (I/I_o)^{\Delta/\Delta'}\right] \quad (9)$$

if $\Delta \approx \Delta'$, equation (4) then reduces to

$$I = I_o - I' \cdot I_o/I'_o \quad (10)$$

Equation (10) may be generalized for the case of several components to

$$\sum_j \frac{I_j}{\sigma_j} = \sum_j \frac{Io_j}{\sigma_{i_o}} - \frac{I' \sum_j Io_j/\sigma_{i_o}}{I'_o} \qquad (11)$$

Setting $\sum_j \frac{I_j}{\sigma_j} = I^T$ (12)

and $\sum_j \frac{Io_j}{\sigma_j} = I_o^T$ (13)

I^T becomes a linear function of I', and in that case it is possible to determine I'_o. Equation (7) may then be used to determine x. This determination is valid only for a composition range where Δ is fairly constant. The experimental values of $\Sigma_j I_j/\sigma_j$ were reasonably constant for the samples, which lends support to the assumptions made above.

In these calculations, Δ = 9.8 Å (515 eV) for Fe_3O_4 was used {12,13}. For the Al 2s and Al 2p photopeaks the escape depth was corrected for kinetic energy using the formula {10}

$$\Delta \propto K^{0,5} \qquad (14)$$

3. RESULTS AND DISCUSSION

3.1 Sapphire samples: Survey Spectra Analysis

Preliminary XPS survey scans of the sapphire samples showed that a thin surface deposit consisting predominantly of iron and chromium was present on regions of the sample that had been exposed to the Tokamak plasma. In comparison to regions that were shielded from the

plasma by the sample mount ($z = 15 - 25$ mm for ion-exposed and $z = 0 - 25$ mm for electron-exposed surfaces), an increase in the C1s signal was observed on the exposed regions of the sample indicating that carbonaceous impurities are present as a plasma pollutant.

The O1s signal was generally lower on surfaces that had been exposed to the Tokamak plasma. However, as will be discussed later (see section 3.4), this observation does not imply that oxygen is not present as a plasma pollutant because the comparison of the O1s intensity for Al_2O_3 (sapphire) and FeO_x or CrO_x depends on the oxide matrix and escape depth.

The observation of the Al2s and Al2p signals from the Al_2O_3 substrate on all samples indicates that the deposit thickness is comparable to the photoelectron mean free path (Δ) of the deposit or that deposition occurs only on limited areas of the sample. This point is discussed in detail in section 3.2. Examples of the survey spectra of exposed and masked regions of a sample are shown in figure 5.

The spectra for the masked regions of the sample compare well with the spectrum of a sapphire sample that was not run in TCA, indicating that molecular and thermal interactions in themselves do not contribute to the changes in the surface composition of the sample.

The conclusion of the analyses may be summarized as follows:

- Regions of the sapphire probes exposed to the plasma are deposited with iron, chromium, some carbon, nickel and possibly oxygen atoms. It is inferred that these atoms are present in the scrape-off region of the plasma. The nature of the transported species may be ions, atoms or clusters.

- Thermal and molecular gas exposure do not result in observable changes of the surface composition of the sample.

3.2 Sapphire samples: Deposit Thickness Determination

In addition to the RBS analysis. the observation of the Al2s and Al2p signals in the XPS survey spectra permit the model described in section 2.5 to be used to determine the overlayer thickness. The thickness of the deposited material was determined for the various samples at 5mm intervals along the radial distance Z using both techniques. Such data are presented in Table 1. A graphical comparison of the depths calculated using RBS as a function of the depths calculated using XPS is shown in figure 6. A least squares fit to the data yielded the relationship·

$$d = 7,59 + 0,97\ d'\ (\text{Å}) \tag{15}$$

where d is the depth calculated using RBS and
d' is the depth calculated using XPS

The coefficient of determination for the fit is 0,88.

The goodness of the fit indicates that models used for both analysis methods are reasonable in view of the fact that the underlying assumptions for the determinations are different. We believe that this comparison is the first quantitative comparison of the XPS and RBS techniques for overlayer thickness determination. It is important to note that the XPS determination is based on the attenuation of the substrate photopeak by the total impurity atoms, whereas the RBS determination is based on the atomic concentration (atoms/cm^2) of the total iron, chromium and nickel content of the deposit. The constant in equation (15) may be explained in terms of carbon contamination which is not detected by the RBS technique.

The deposit thicknesses as a function of radial distance Z are shown in figures 7-10. Figures 7 and 8 are the RBS data and figures 9 and 10 are the XPS data. Figures 7 and 9 are for samples 30.6.80 - 8.9.80 and figures 8 and 10 are for samples 8.9.80 - 22.11.80.

It is clear that the deposit thickness is highest in sector 7,8 exposed to the ion flux. The limiter is situated in sector 9 (see figure 3) indicating that the impurity fluxes of metallic particles originate from the limiter which is constructed of 304-stainless steel. Samples from sector (7,8) (i.e. close to the limiter) show a pronounced anisotropy as regards the deposit thickness on the "electron side" compared with the "ion side" of the sample surfaces. This clearly indicates that, at the sample position in sector (7,8), the impurity fluxes in the ion current direction are higher than those in the electron current direction. The deposit thickness on the "electron side" of the sample is comparable to the almost isotropic deposit thickness measured at the electron and ion sides of samples from sector (16, 17) which is situated at a certain distance from the limiter.

These observations suggest that interaction of suprathermal electrons with the limiter is the main mechanism for erosion and impurity release. Accordingly, the "ion side" of the sample in sector (7,8) receives an additional anisotropic flux of impurities released from the limiter whereas the "electron side" of the sample in sector (7,8) and both sides of the sample from sector (16,17) receive an essentially isotropic flux.

The observed nonuniform deposit thickness as a function of radial distance lends support to the conclusion that the limiter is the source of the contamination (i.e. less material is deposited close to the first wall). In general, the highest deposition occurs near the plasma edge (z = 45 - 50mm), except for the ion-exposed surface from sector (16,17), which shows a maximum at z = 40 mm.

From the deposit thickness data it is possible to make a comparison of the deposition rates of metallic impurities for other Tokamak devices. From the RBS data for the samples from position (7,8) on the ion-exposed surfaces the deposition rate is 5-10 x 10^{14} atoms/cm^2-discharge for iron plus chromium atoms. This value may be compared with the following data: 8×10^{13} Ni for D-111, 2×10^{14} Mo for TFR400, 1×10^{15} Ni for TFR600, 1×10^{13} Fe for PULSATOR, 3×10^{12} Fe for DITE and 5×10^{14} Mo for ALCATOR. The data for TCA agree well with these values.

As discussed by Smith {5}, such a comparison may be difficult to analyse quantitatively because of the decay lengths of impurities in the plasma edge and the limiter probe distance. From our data it is clear that strong gradients in the deposition exist in the radial and azimuthal directions and, therefore, care should be exercised in this comparison. Further research is also required to establish the influence of erosion processes that may occur simultaneously with deposition at the sample surface {5}.

3.3 Stainless Steel Samples: Substrate Compositional Changes

In this section the possible changes in composition of the stainless steel substrate are determined. In the absence of deposition, the observed differences in the XPS spectra for exposed and unexposed samples directly relate to this effect. However, if deposition is considered as an additional process it is necessary to subtract the contribution of this overlayer from the spectra for the exposed sample. The parameter of interest in this analysis is the Fe/Cr atomic ratio and how this parameter changes in the substrate steel surface region.

We assume that the 'sister' sapphire sample provides the correct Fe/Cr ratio and depth of the deposit on the steel sample (i.e. that deposition is independent of substrate and that the deposit and steel substrate do not interdiffuse).

In that case the deposit consists of a layer with a Fe/Cr ratio equal to that measured for the sapphire sample, R_s, extending as a uniform layer to a depth X, which is the depth determined from data for the sapphire sample. The measured atomic ratio for the steel sample is R_m.

For the case where no segregation or change in the surface Fe/Cr ratio occurs in the stainless steel substrate, the relative contribution, a, of the overlayer may be expressed by

$$a = e^{-x/\Delta \sin\Theta} \qquad (16)$$

and for the substrate the contribution, b, may be expressed

$$b = (1 - e^{-x/\Delta\sin\Theta}) \tag{17}$$

where

$$a + b = 1. \tag{18}$$

The theoretical ratio of Fe/Cr, R_T, is calculated using the equation

$$R_T = aR_s + bR_c, \tag{19}$$

where R_C is the Fe/Cr ratio measured for an unexposed stainless steel sample.

If $R_m \sim R_T$, then it is reasonable to assume that no significant changes occur in the Fe/Cr atomic ratio of the steel substrate.

Calculations of R_T and R_m were performed. The general conclusion reached is that the observed Fe/Cr ratio in the surface region may be explained in terms of the relative contributions of the Fe/Cr ratio of the deposit and of the steel substrate. This indicates that segregation of the steel substrate does not occur and that the steel sample behaves as a deposition substrate only.

It should be noted that the value of R_T is only semiquantitative and that segregation effects, which are of a small magnitude, cannot be resolved. In general, this estimate is of greatest value for thin overlayers of deposited material. When $d > \Delta$ then the value of this analysis is doubtful.

3.4 XPS Analysis of the Deposit

Figures 11 to 16 show the ratio of the Fe2p, Cr2p, C1s photopeak areas (or heights) to the O1s photopeak area (or height) as a function of Z for a selection of the various surfaces studied. Also shown in these figures is theFe2p/Cr2p photopeak area ratio. The latter data is summarized in figure 17.

It is clear from the data that the elemental composition of the samples show striking variations (in particular, the Fe/Cr ratio). The complexity of the results do not permit a clear interpretation and further research is required to establish the underlying mechanisms for these variations. However, the Fe/Cr ratio shows a definite maximum at Z = 25 - 40 mm for the ion-exposed surface of samples from sector (7,8) and this effect is less pronounced for samples from sector (16, 17).

Atomic compositions of various samples are shown in table 2: the Fe/Cr ratios deviate significantly from the bulk composition of the wall or limiter material. In general, the Fe/Cr atomic ratio is significantly higher than the bulk composition.

Some speculations regarding the source of these inhomogeneities are:

a) Studies on plasma-surface interaction using a DC discharge in a special chamber made of stainless steel have demonstrated that material sputtered from the wall and deposited on a probe at floating potential is enriched in iron as compared to the original composition of the wall material.

b) Preferential sputtering of one element from the surface.

c) Selective transport through the plasma (mass spectrometer type effect).

Process (c) is probably of some importance because the Fe/Cr atomic

ratio shows both strong radial and angular dependences for the sapphire samples.

In the region of maximum deposition ($Z \sim 40$ mm) the sapphire samples show a decrease in the intensity of the O1s peak; however, the stainless steel probes show an increase in the O1s peak intensity. This suggests that the deposit is oxidized to a greater extent than the unexposed stainless steel surface, which indicates that oxygen is present as an impurity in the Tokamak plasma <u>or</u> that oxidation of the deposit occurs during transport and removal of the sample.

3.5 Chemical Environment of the Species Deposited

Detailed spectra of the Fe2p and Cr2p core levels of the deposit on sapphire revealed that both elements are in an oxide-type environment and that a metallic component is absent from the spectra. This lends support to the conclusion that the deposited material is in an oxide environment.

For the stainless steel samples before exposure, a metallic and an oxide contribution were present for iron and an oxide contribution for chromium.

It is important to reiterate that oxidation of the deposit during sample transport and removal may be responsible for the oxidized state of the deposit and that further in-vacuo studies are required to ascertain the importance of oxygen as a plasma pollutant.

4. CONCLUDING REMARKS

As one may predict from previous studies on other Tokamak devices, the principal impurity detected in the TCA-plasma scrape-off layer is iron and chromium metal. It is concluded that the limiter is the dominant source of metallic contaminants and that suprathermal electrons ("runaway" electrons) are responsible for the largest part of the erosion process. The erosion-transport-deposition mechanism is not well understood. However, from the present study it is clear that large gradients in both composition and depth exist as regards radial and angular dependence of the deposited material in the torus.

With respect to the depth profiles in the radial direction it is concluded that deposition is greater towards the plasma edge compared with the near-wall region. This agrees with the expected trend, however, some samples show departures from this behaviour and the possibility of simultaneous erosion of the samples should be investigated. Studies at TFR have demonstrated that the deposit thickness increases in the wall to plasma-edge direction and then decreases close to the plasma edge which demonstrates that maxima exist in the overall deposition rate in the boundary layer. Surfaces of the probes near the limiter exposed to the direction of the ion-flux (sector (7,8)) show a anisotropy as regards deposition on both of the sample surfaces: Deposition is markedly higher on the ion current side. This is explained by interaction of suprathermal electrons ("runaway electrons") with the limiter being the main source of the limiter erosion and impurity release.

The compositional inhomogeneity along the radial axis ofthe samples suggests that, amongst other possibilities, selective transport is of some importance.

From this study the presence of oxygen as a plasma pollutant cannot be excluded. Detailed experiments using an in-vacuo sample transfer mechanism are required to permit a shot-by-shot study in an oxygen free environment. This type of experiment should also permit investigation of the importance of sample erosion.

Finally, the deposition rate of metallic impurities per shot compares well with existing data for other Tokamaks. However, we have demonstrated that the spatial inhomogeneity of the deposited materials does not support the value of single measurements on one region of the torus only and that caution should be exercised in the comparison with existing data which is limited to single proble measurements.

REFERENCES

{1} G.M. McCracken and P.E. Stott: Nuclear Fusion 19, (1979), 889

{2} A.D. Cheetham, A. Heym, F. Hofmann, K. Hruska, R. Keller, A. Lietti, J.B. Lister, A. Pochelon, H. Ripper, R. Schreiber and A. Simik: "The TCA Tokamak Project Report 1979", LRP 162/80, Ecole Polytechnique Fédérale de Lausanne-Suisse

{3} J.K. Howard, W.K. Chu and R.F. Lever: "Ion Beam Surface Layer Analysis", O. Meyer, G. Linker and F. Käppeler (eds.) Vol. 1, p. 125. New York: Plenum Press 1975

{4} H.F. Dylla and S.A. Cohen, J. Vac. Sci. Technol. 14, (1977), 565

{5} J.N. Smith and C.H. Meyer, J. Vac. Sci. Technol. 19, (1981), 63

{6} Ph. Staib and G. Staudenmaier, J. Nucl. Mat. 63, (1976), 37

{7} G.M. Mc Cracken and D.H.J. Goodall, Nucl. Fusion 18, (1978), 537

{8} L.C. Emerson, R.E. Clausing and L. Heatherly, J. Nucl. Mat. 76/77 (1978), 472

{9} J.K. Gimzewski, Ph.D. Thesis, University of Strathclyde (1974)

{10} C.D. Wagner, Anal. Chem. 49, (1977), 1282

{11} J.H. Scofield, J. Electron Spectrosc. 8, (1976), 129

{12} C.J. Powell, Surf. Sci. 44, (1974), 29

{13} P.B. Needham and T.J. Driscoll, J. Vac. Sci. and Technol. 11, (1974), 278

{14} J.K. Gimzewski and S. Veprek: unpublished data

TABLES

Table 1: Depth of material deposited on sapphire probes calculated from XPS and RBS data

Table 2: Composition analysis of various samples (30.6.80 - 8.9.80) determined by XPS and bulk compositions of Tokamak wall and limiter.

Table 1

Depth of material deposited on sapphire probes calculated from XPS and RBS data.

Sample/ Sector Position/ Surface	Analysis Position Z(mm)	Deposit Thickness (Å)	
		RBS	XPS
30.6.80-8.9.80/ (7,8)/ ION	48	45,2	-
	45	39,7	39,3
	40	26,0	39,4
	35	18,6	20,1
	30	7,8	12,7
	25	2,1	9,8
30.6.80-8.9.80/ (7,8)/ ELECTRON	48	11,7	-
	45	10,5	18,2
	40	3,2	11,3
	35	1,8	2,3
	30	0,5	0,0
30.6.80-8.9.80/ (16,17)/ ION	48	7,6	-
	45	7,5	16,4
	40	6,6	14,0
	35	2,2	9,7
30.6.80-8.9.80/ (16,17)/ ELECTRON	45	5,8	
8.9.80/22.11.80/ (7,8)/ ION	5		0,1
	13		0
	28	7,0	-
	30	6,7	13,6
	35	16,0	30,3
	40	22,5	38,1
	45	40,5	45,2
	49	48,4	-
8.9.80/22.11.80/ (7,8)/ ELECTRON	30	1,7	
	35	2,2	
	40	4,1	
	45	15,1	
8.9.80/22.11.80/ (16,17)/ ION	5	0	
	22	0,4	
	25	2,6	
	30	2,3	
	35	5,5	
	40	18,0	
	45	4,8	
	47	3,3	
8.9.80/22.11.80/ (16,17)/ ELECTRON	5	0,3	
	22	0,3	
	35	1,6	
	40	9,2	
	45	12,2	
	47	11,3	

Table 2

Sample 30.6.-8.9.80	SECTOR	POSITION (mm)	ATOMIC PERCENT COMPOSITION * O	Cr	Fe	Ni	Mo	C	N	Mn	ATOMIC RATIO Fe/Cr	Fe/Ni
Stainless steel (ion-exposed)	16,17	10	38,5	27,5	32,0	0,4	1,7	28,0	10,3	-	1,16	
	"	40	41,6	24,8	37,7	1,3	1,1	32,2	2,9	-	1,52	
Stainless steel (ion-exposed)	7,8	10	40,7	36,7	34,5	2,8	-	21,6	5,0	-	0,94	
		30	74,3	13,7	46,8	-	-	39,5	0	-	3,42	
		45	56,5	39,4	22,2	-	-	31,1	7,3	-	0,56	
Sapphire (ion-exposed)	7,8	35	68,7	8,0	54,8	0,2	0,6	36,5	0	-	6,85	
		40	50,9	9,3	40,8	0,2	0,4	29,9	19,3	-	5,47	
Sapphire (ion-exposed)	16,17	40	110	21	21	0	0	55	2	-	1,0	
Bulk Composition of SS304+	(limiter)	-	-	18-20	71-65	8-12	-	-	-	2	3,93 - 3,25	8,86 - 5,4
Bulk Composition of SS316LN[a]	(first wall)			16,5 - 18,5	60 - 66	12 - 14,5	2,5- 3,5	-	-	-	3,25 - 3,98	4,2 - 5,6
Stainless steel 316 LN Argon Etched				-	-	-	-	-	-	-	3,64	3,18

* - Atomic percent of total atoms detected, excluding oxygen

\+ - CRC Chemistry and Physics Handbook

a - Information from EIR Würenlingen

FIGURES CAPTIONS

Figure 1 Sample Geometry of the TCA probe with samples inserted

Figure 2 Sample Geometry in relation to the TCA Tokamak radial plasma dimensions

Figure 3 Positions of the probes and limiter on the TCA Tokamak

Figure 4 Example of the Fe,Cr and Ni peaks in a typical RBS spectrum

Figure 5 Example of the XPS survey spectra for an exposed region and unexposed region of a sapphire sample

Figure 6 A comparison of the deposit thickness determined from RBS data as a function of the deposit thickness determined from XPS data. Solid line is a linear least squares fit to the data

Figure 7 Deposit thickness as a function of radial distance Z for sapphire sample 30.6.80-8.9.80 determined by RBS

Figure 8 Deposit thickness as a function of radial distance Z for sapphire sample 8.9.80-22.11.80 determined by RBS

Figure 9 Deposit thickness as a function of radial distance Z for sapphire sample 30.6.80-8.9.80 determined by XPS

Figure 10 Deposit thicknesses as a function of radial distance Z for sapphire sample 8.9.80-22.11.80 determined from XPS data

Figure 11 Peak height ratios of the $Fe2p^{3/2}$/O1s, $Cr2p^{3/2}$/O1s, C1s/O1s and $Fe2p^{3/2}$/$Cr2p^{3/2}$ photopeaks as a function of radial distance Z for the ion-exposed surface of stainless steel sample 8.9.80-22.11.80 from sector (7,8)

Figure captions (cont'd)

Figure 12 Peak height ratios of the $Fe2p^{3/2}/O1s$, $Cr2p^{3/2}/O1s$, C1s/O1s and $Fe2p^{3/2}/Cr2p^{3/2}$ photopeaks as a function of radial distance Z for the ion-exposed surface of sapphire sample 8.9.80-22.11.80 from sector (7,8)

Figure 13 Peak area ratios of the Fe2p/O1s. Cr2p/O1s. C1s/O1s and Fe2p/Cr2p photopeaks as a function of radial distance Z for the ion-exposed surface of stainless steel sample 30.6.80-8.9.80 from sector(7,8)

Figure 14 Peak area ratios of the Fe2p/O1s, Cr2p/O1s. C1s/O1s and Fe2p/Cr2p photopeaks as a function of radial distance Z for the ion-exposed surface of sapphire sample 30.6.80-8.9.80 from sector(7,8)

Figure 15 Peak area ratios of the Fe2p/O1s, Cr2p/O1s, C1s/O1s and Fe2p/Cr2p photopeaks as a function of radial distance Z for the ion-exposed surface of stainless steel sample 30.6.80-8.9.80 from sector (16,17)

Figure 16 Peak area ratios of the Fe2p/O1s, Cr2p/O1s, C1s/O1s and Fe2p/Cr2p photopeaks as a function of radial distance Z for the ion-exposed surface of sapphire sample 30.6.80-8.9.80 from sector (16,17)

Figure 17 Peak area ratios of the Fe2p/Cr2p photopeaks as a function of radial distance for the ion-exposed surfaces of samples 30.6.80-8.9.80

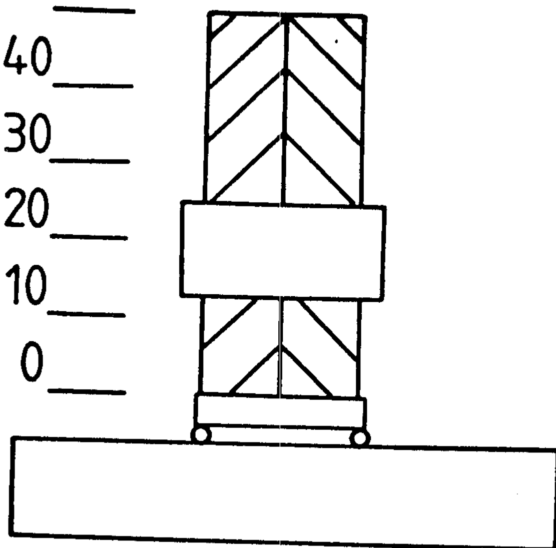

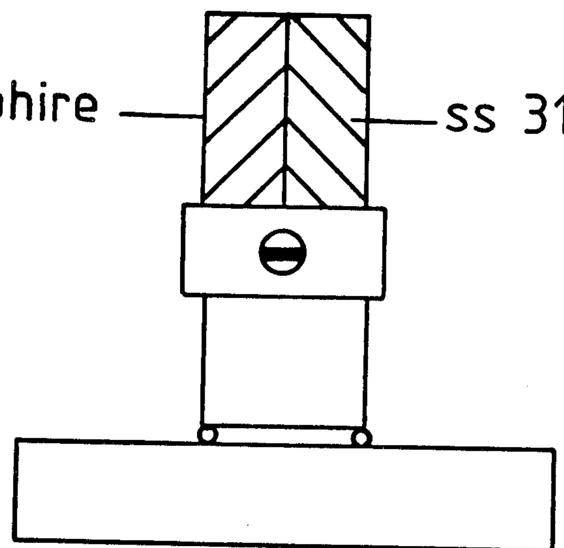

Hatched areas show sample area exposed to plasma

Figure 1

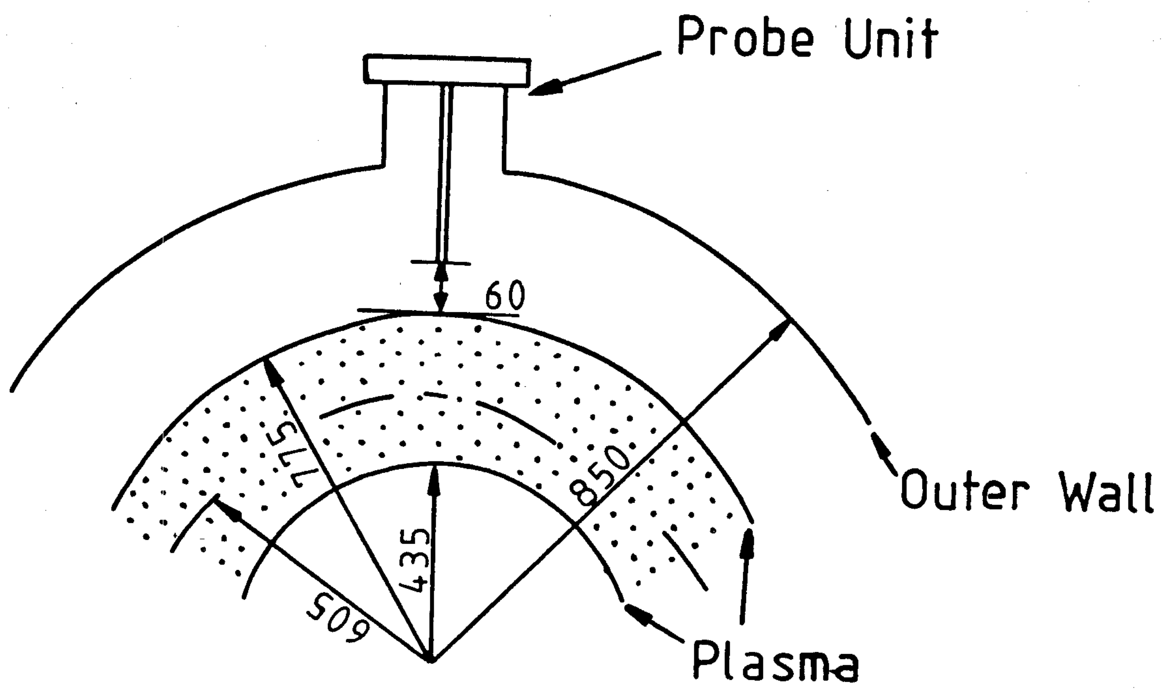

dimensions in mm

Figure 2

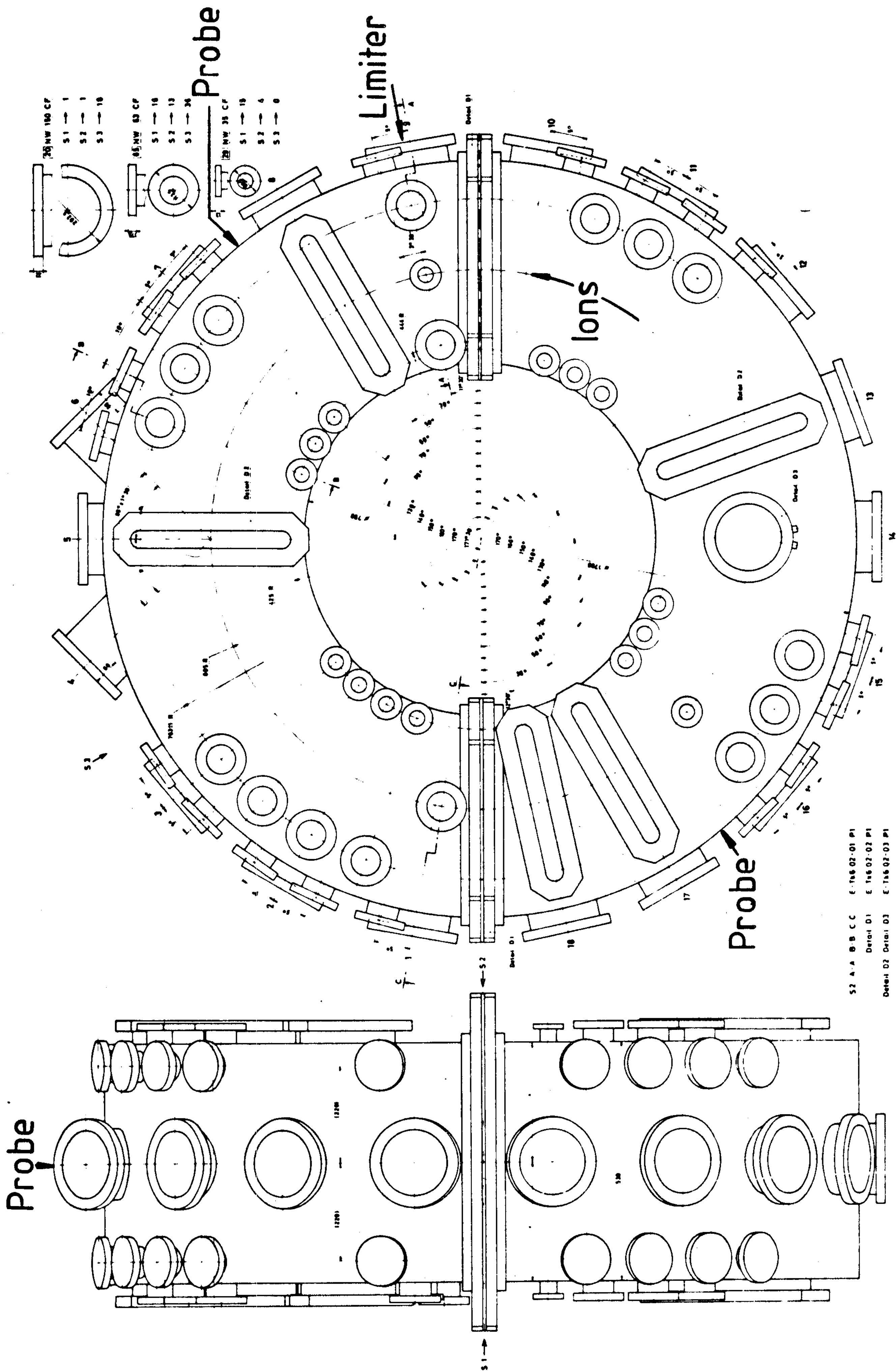

Figure 3

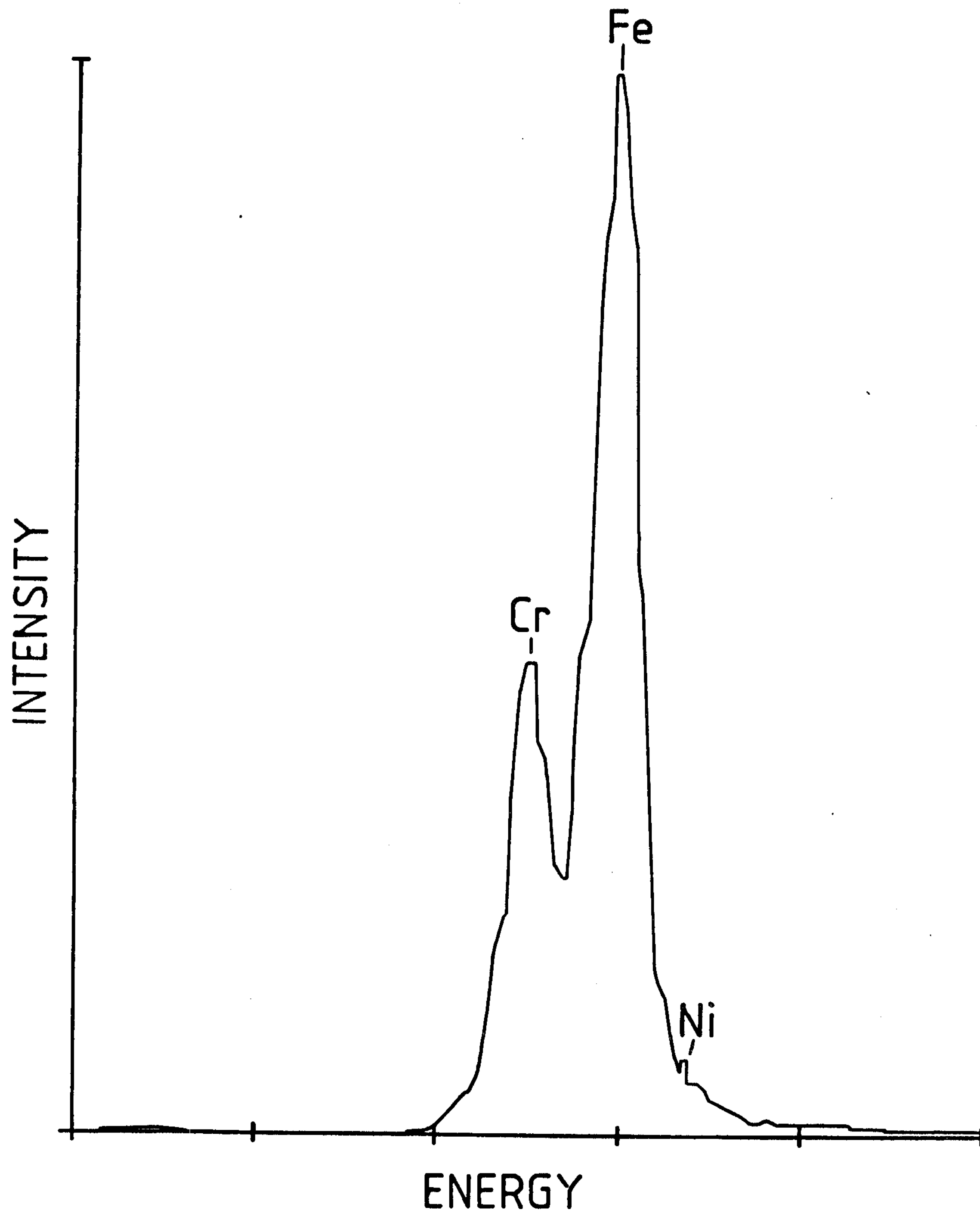

Figure 4

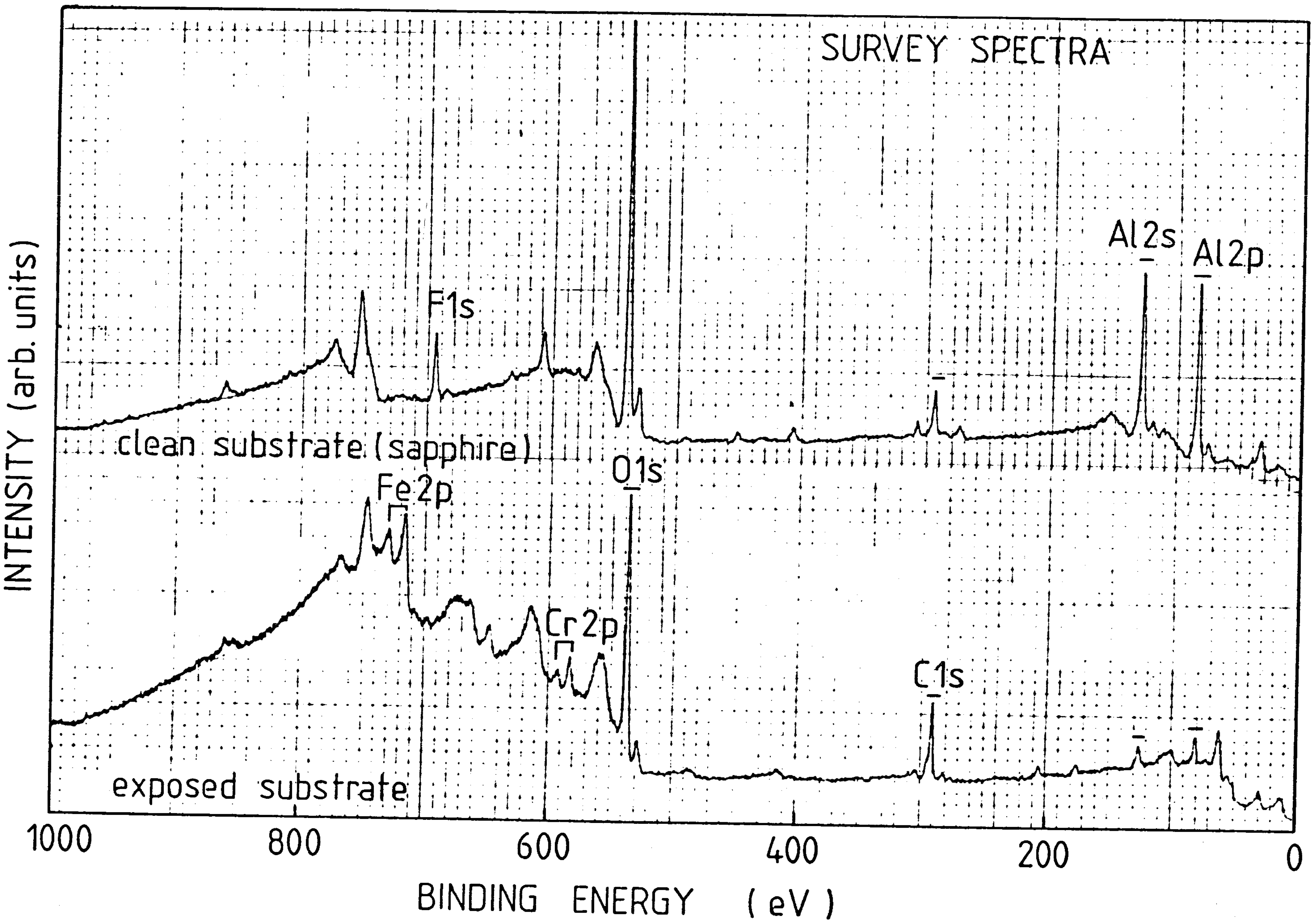

Figure 5

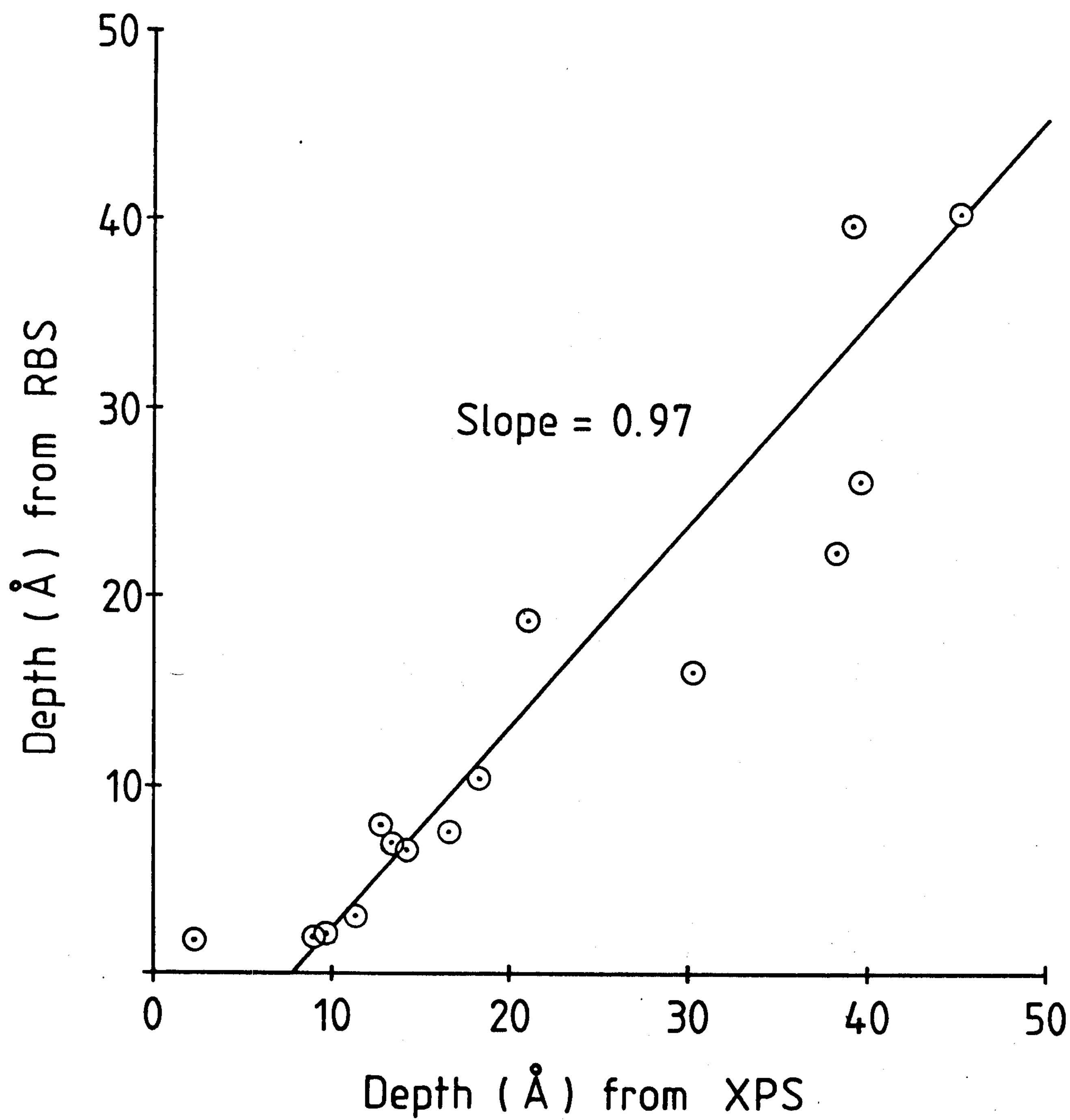

Figure 6

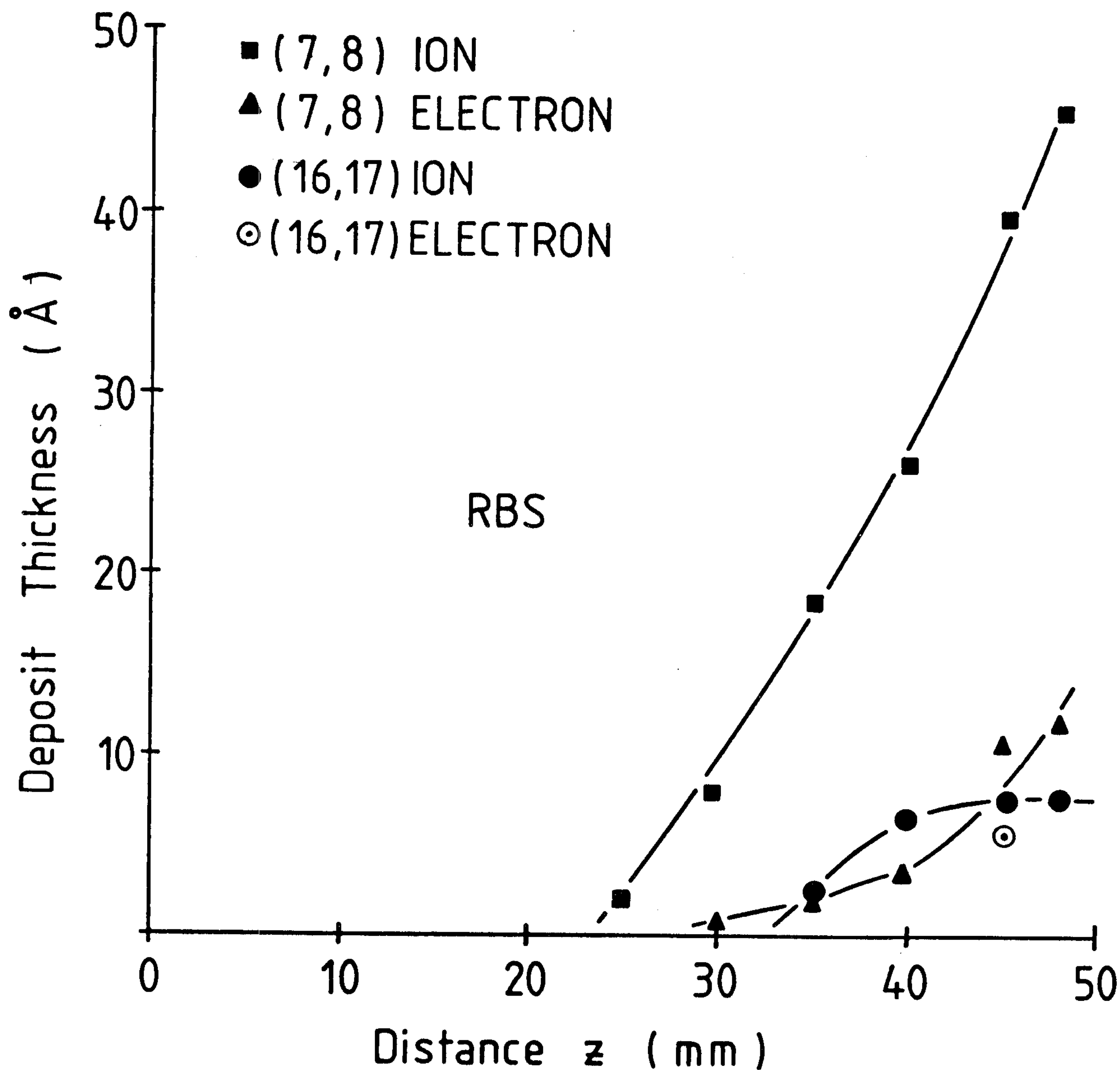

Figure 7

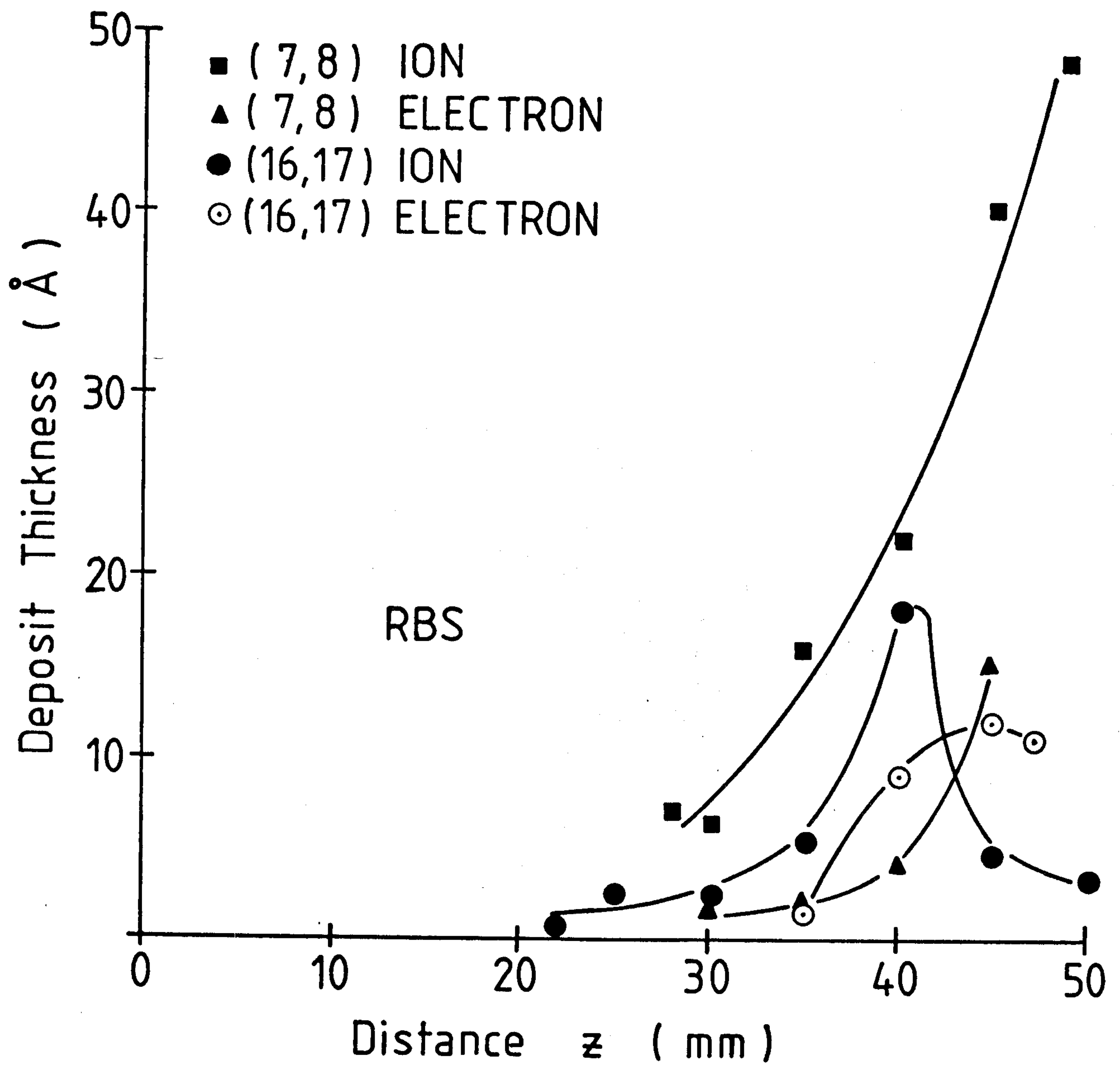

Figure 8

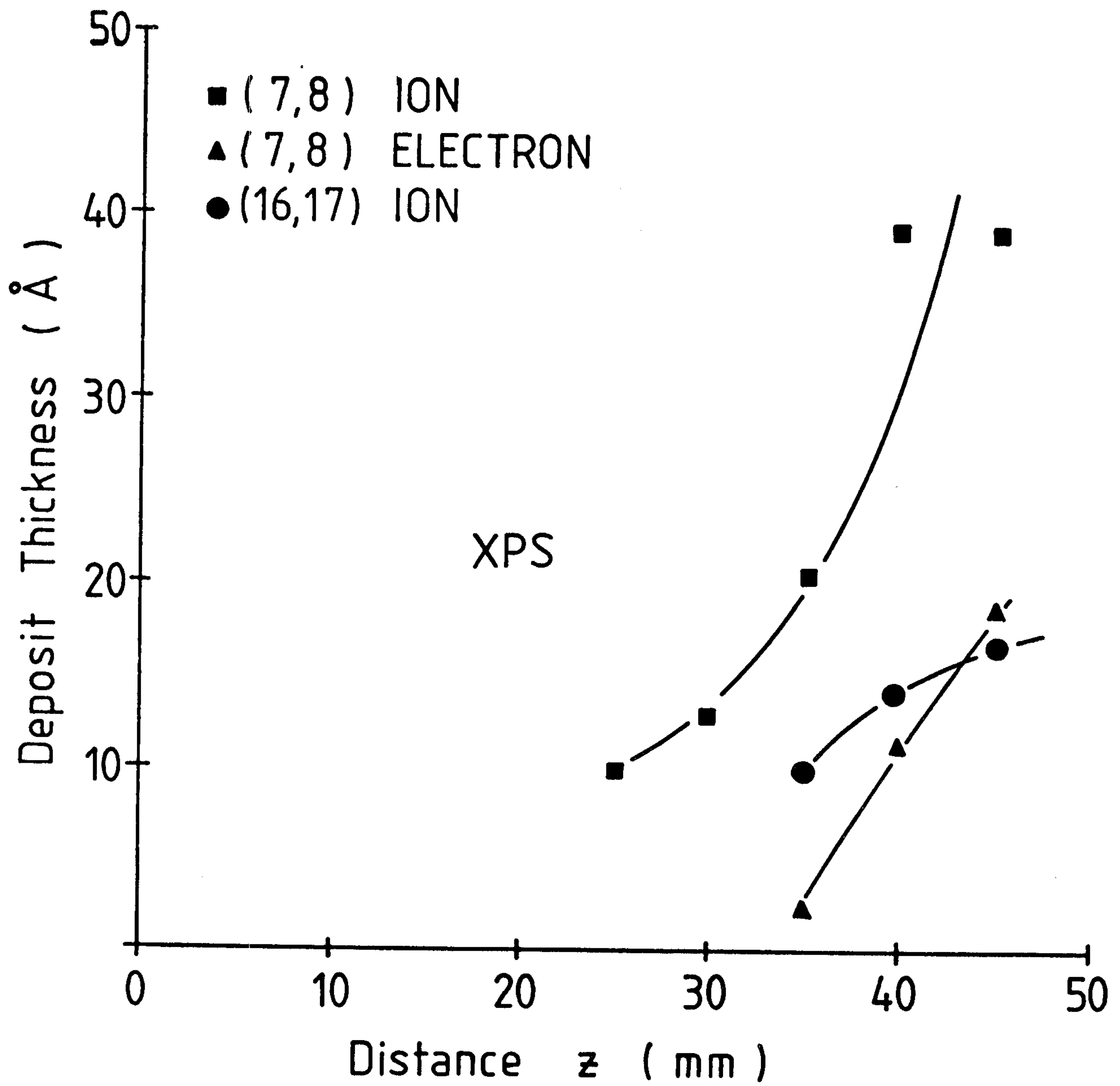

Figure 9

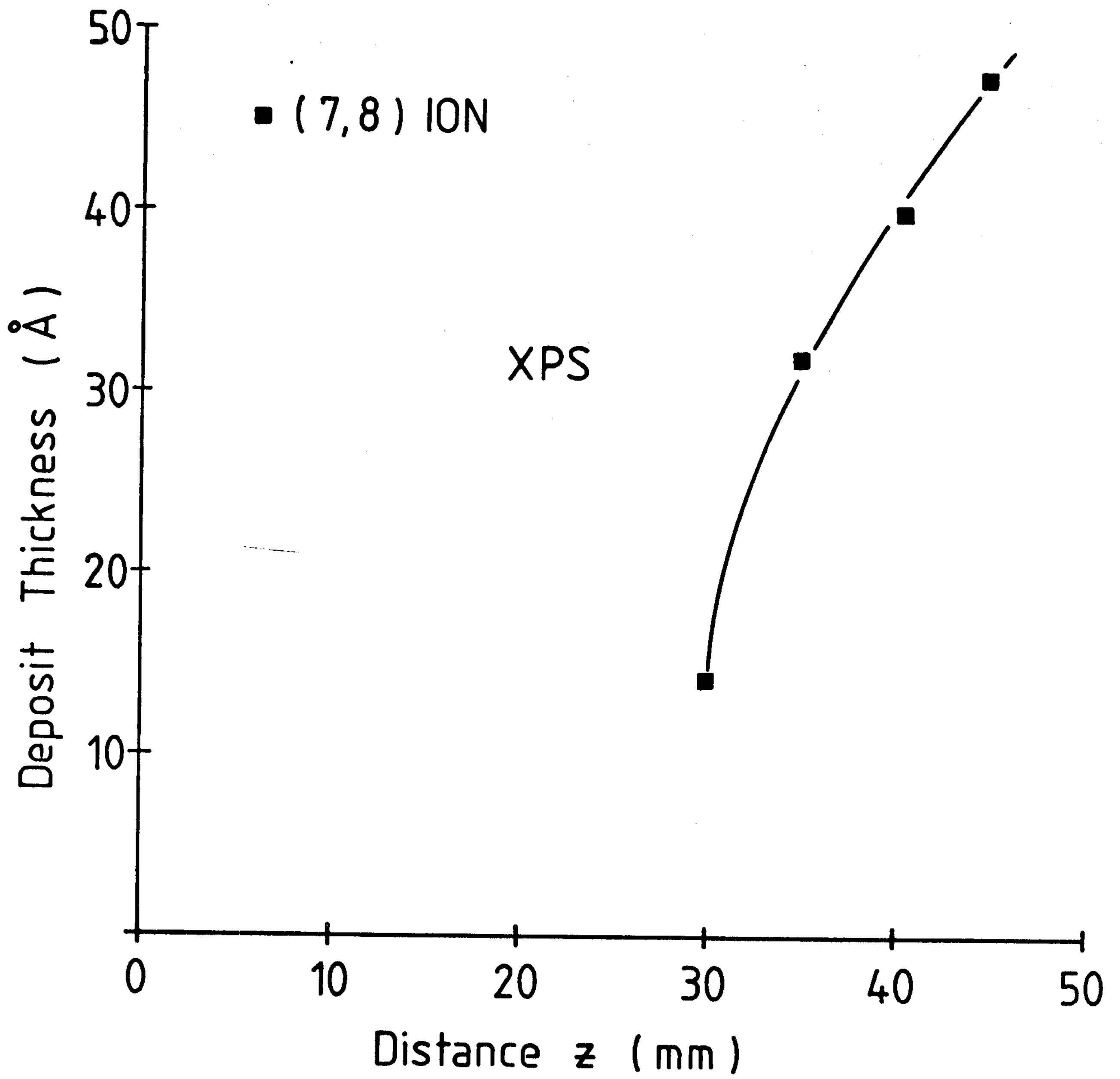

Figure 10

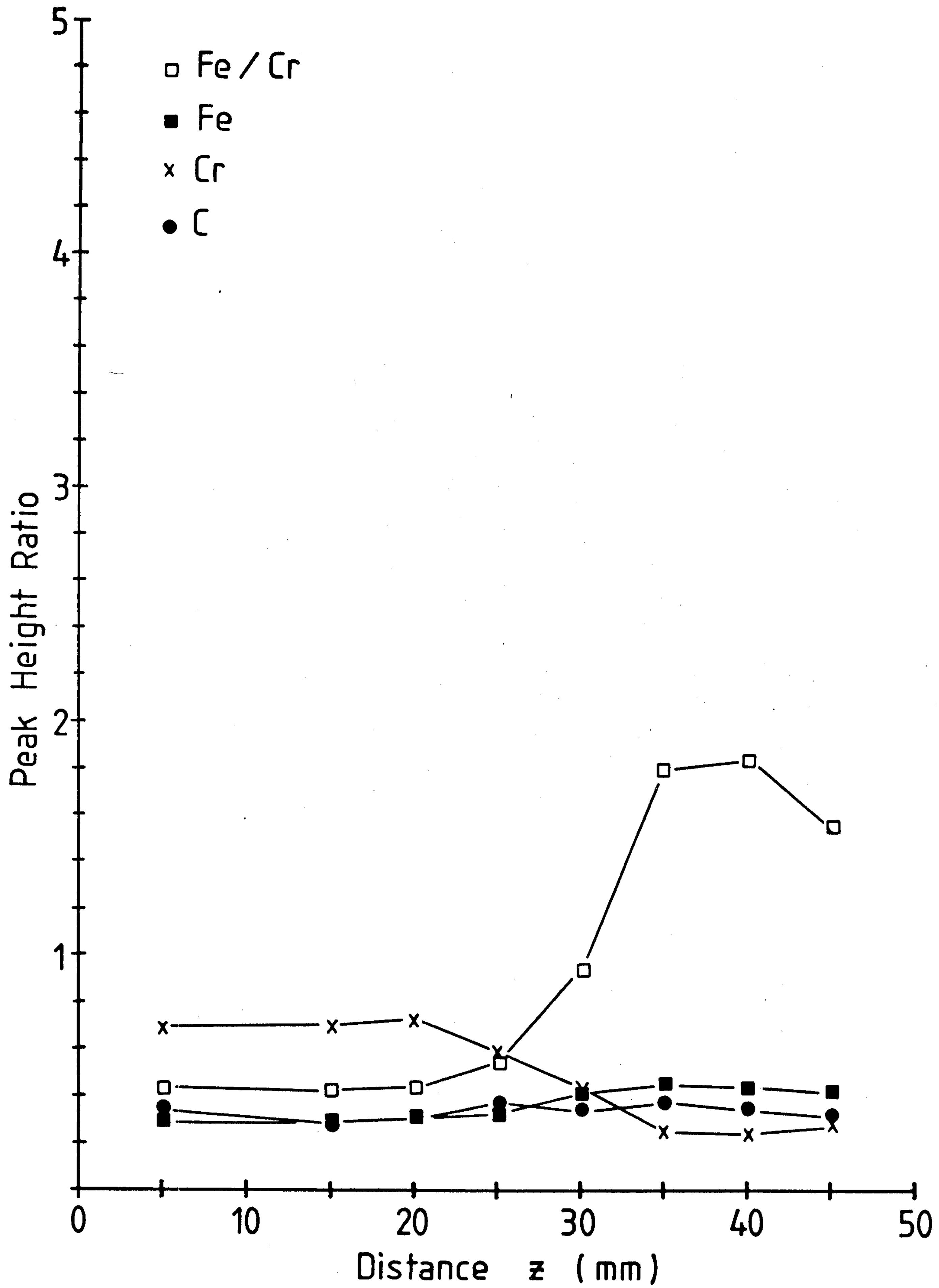

Figure 11

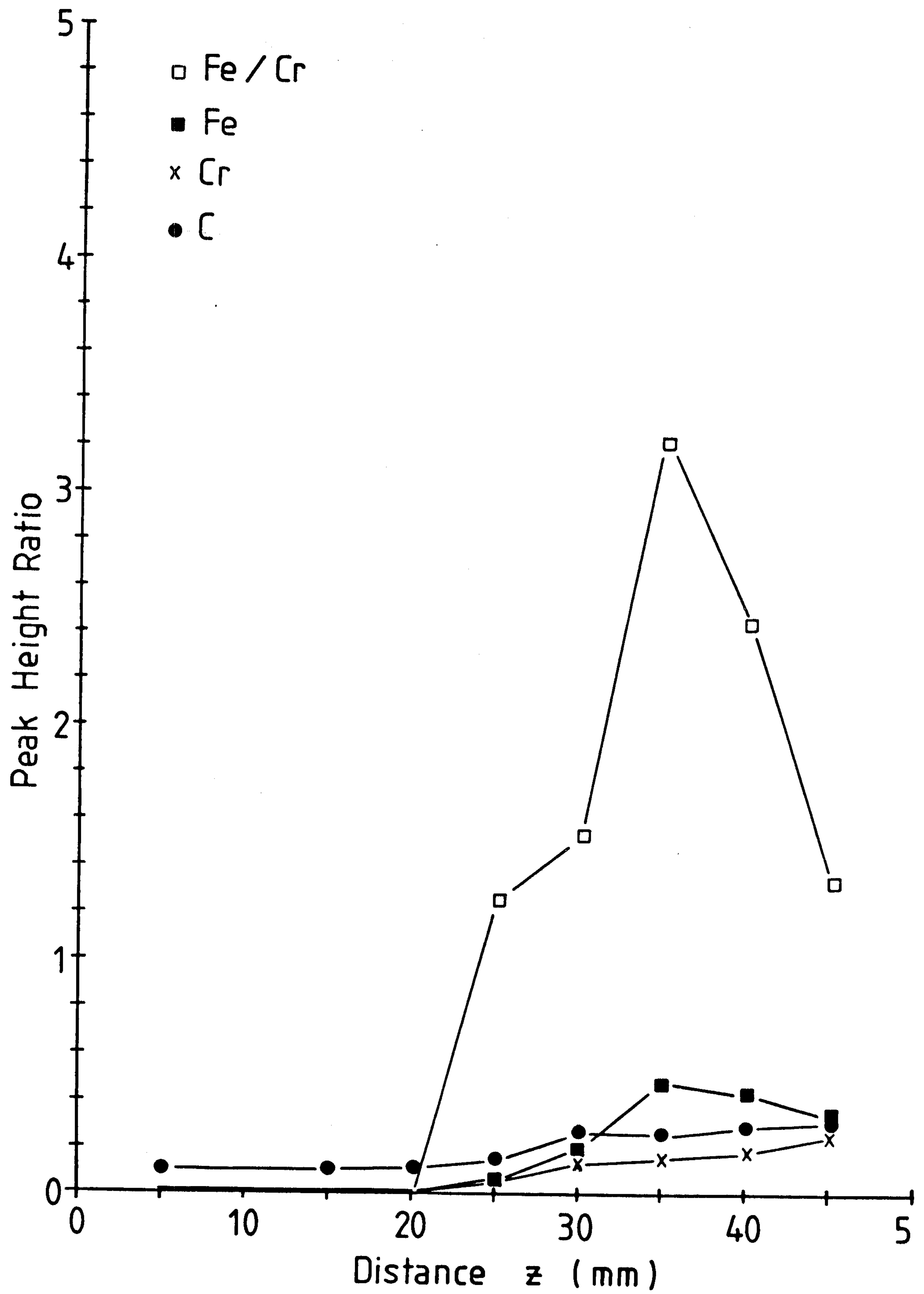

Figure 12

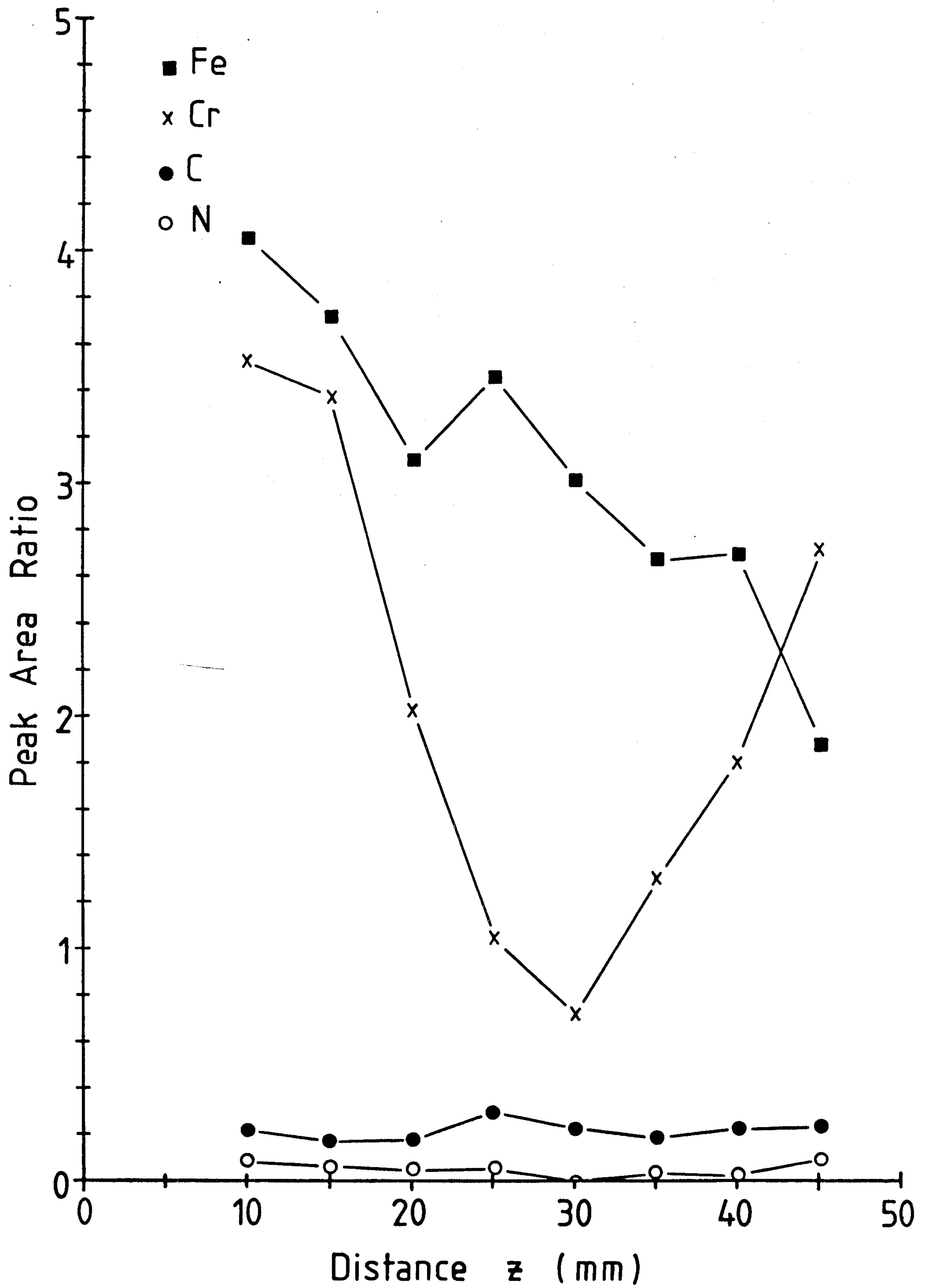

Figure 13

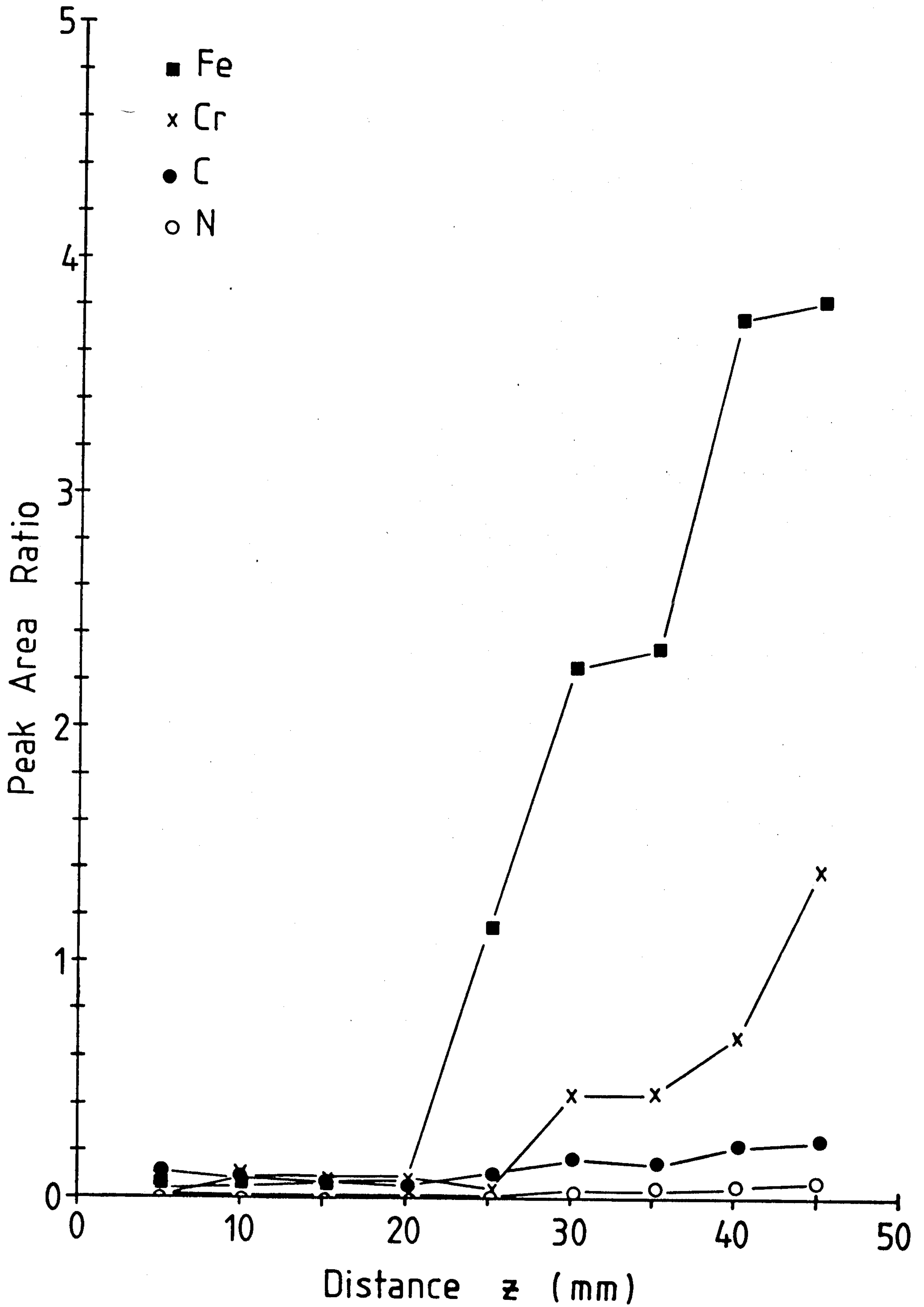

Figure 14

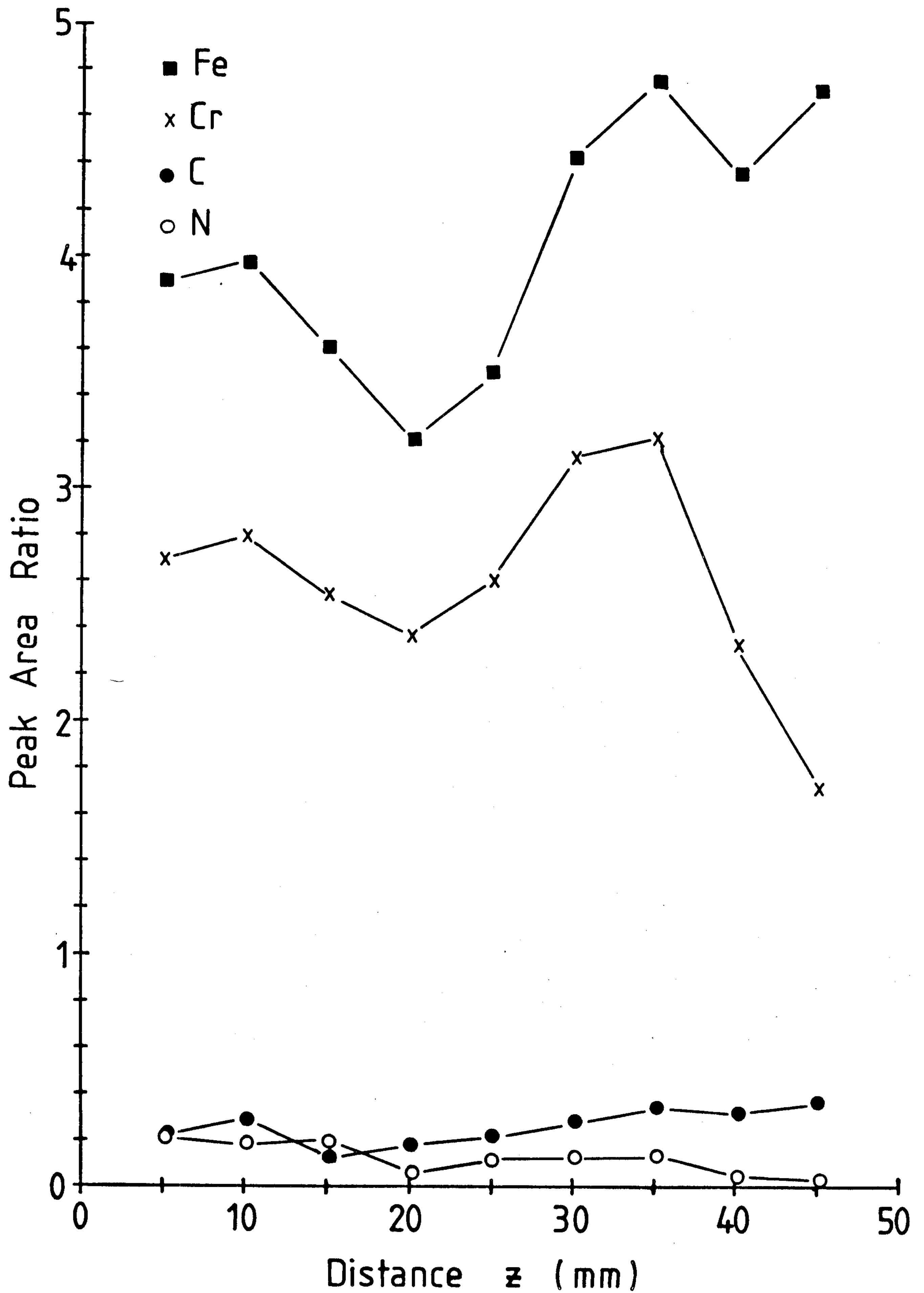

Figure 15

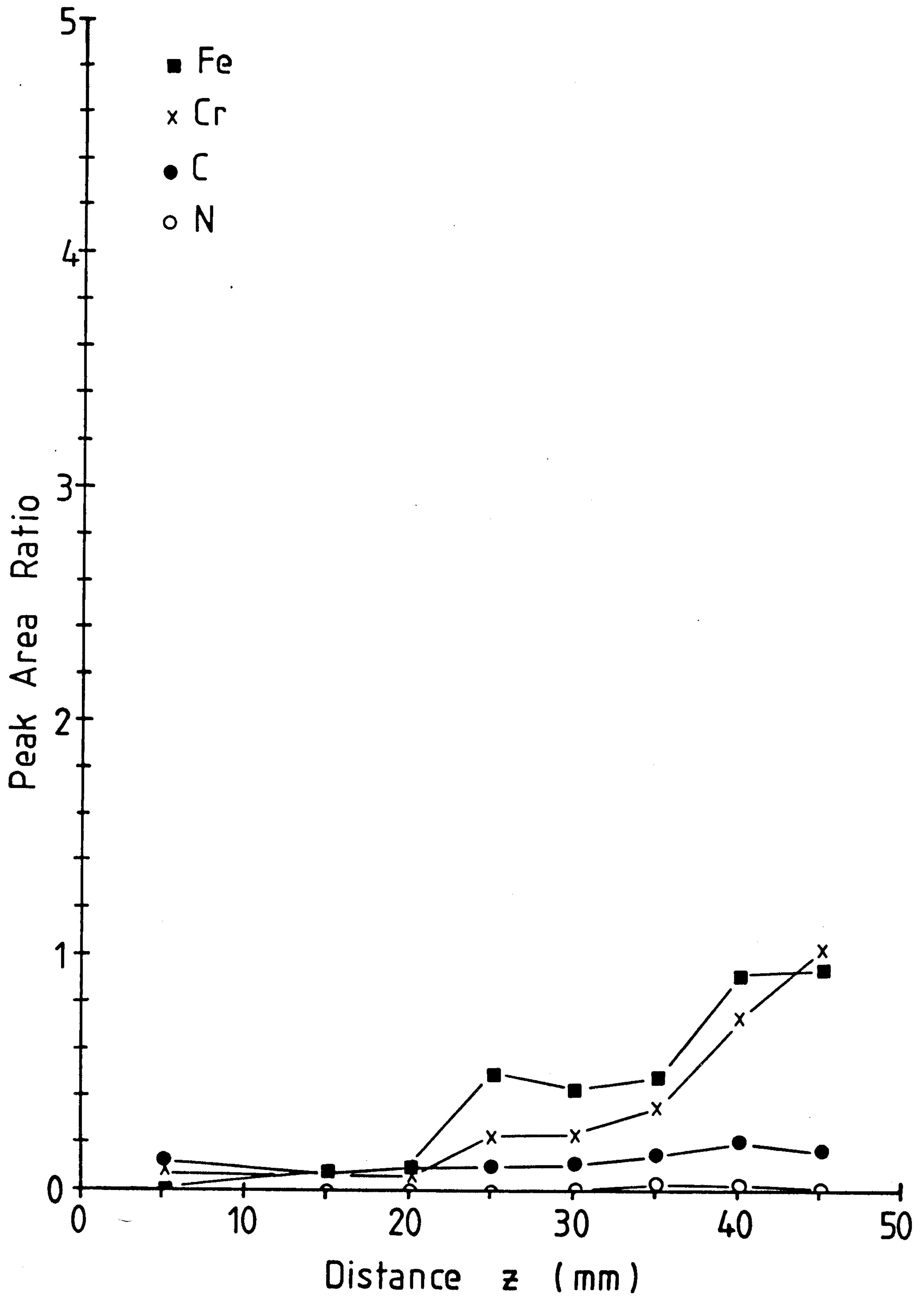

Figure 16

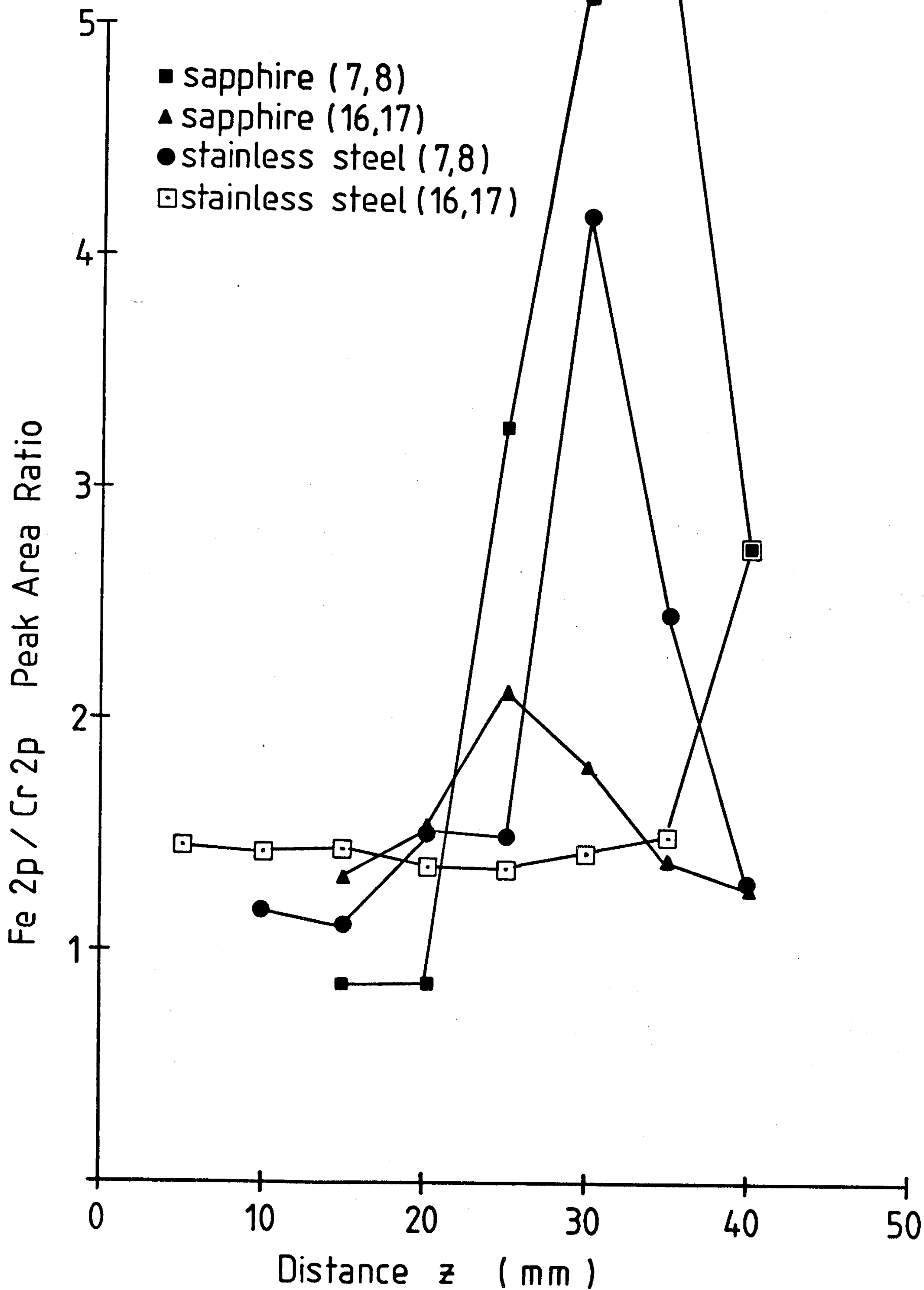

Figure 17